SUPPORTING INFORMATION

Entry from the lipid bilayer: a possible pathway for inhibition of a peptide G protein-coupled receptor by a lipophilic small molecule

Michael P. Bokoch[1,2], Hyunil Jo[3], James R. Valcourt[4#], Yoga Srinivasan[1], Albert C. Pan[4], Sara Capponi[1], Michael Grabe[1], Ron O. Dror[4‡], David E. Shaw[4,5], William F. DeGrado[3], and Shaun R. Coughlin[1*]

[1]Cardiovascular Research Institute, University of California, San Francisco, CA 94158;
[2]Department of Anesthesia and Perioperative Care, University of California, San Francisco, CA 94143;
[3]Department of Pharmaceutical Chemistry, University of California, San Francisco, CA 94143;
[4]D. E. Shaw Research, New York, NY 10036;
[5]Department of Biochemistry and Molecular Biophysics, Columbia University, New York, NY 10032, USA

Current addresses: [#]Systems Biology PhD Program, Harvard University, Cambridge, MA 02138;
[‡]Departments of Computer Science, Structural Biology, and Molecular and Cellular Physiology, and the Institute for Computational and Mathematical Engineering, Stanford University, Stanford, CA 94305

[*]To whom correspondence should be addressed: Cardiovascular Research Institute, University of California, San Francisco, 555 Mission Bay Blvd South, San Francisco, CA 94158. Tel.: (415) 502-8667; Fax: (415) 476-8173; E-mail: Shaun.Coughlin@ucsf.edu.

SUPPORTING FIGURES AND CAPTIONS:

FIGURE S1. **Trajectories of vorapaxar COM during TAMD simulations of vorapaxar dissociation from PAR1.**

FIGURE S2. **Heterogeneity of metastable states prior to extracellular exit.**

FIGURE S3. **Vorapaxar-PAR1 interactions in the TM6-7 metastable state.**

FIGURE S4. **Vorapaxar-lipid interactions in the TM6-7 metastable state.**

FIGURE S5. **UV absorption spectroscopy of vorapaxar.**

FIGURE S6. **Phosphoinositides accumulation assay.**

FIGURE S7. **Cell surface expression of N-terminally FLAG tagged human PAR1 (hPAR1).**

FIGURE S8. **Calcium flux inhibition assay of Rat1 fibroblasts stably expressing hPAR1.**

FIGURE S9. **Effect of vehicle on calcium fluorescence assay in Rat1 fibroblasts stably expressing hPAR1.**

FIGURE S10. **Inhibition of calcium flux in response to 3 μM SFLLRN by vorapaxar derivatives in Rat1 fibroblasts stably expressing hPAR1.**

SUPPORTING MOVIES AND CAPTIONS:

MOVIE S1. **Representative MD simulation of vorapaxar extracellular exit.**

MOVIE S2. **Representative MD simulation of vorapaxar exit through TM6-7.**

MOVIE S3. **Representative MD simulation of vorapaxar exit through TM4-5.**

MOVIE S4. **Calcium flux induced by PAR1 agonist SFLLRN.**

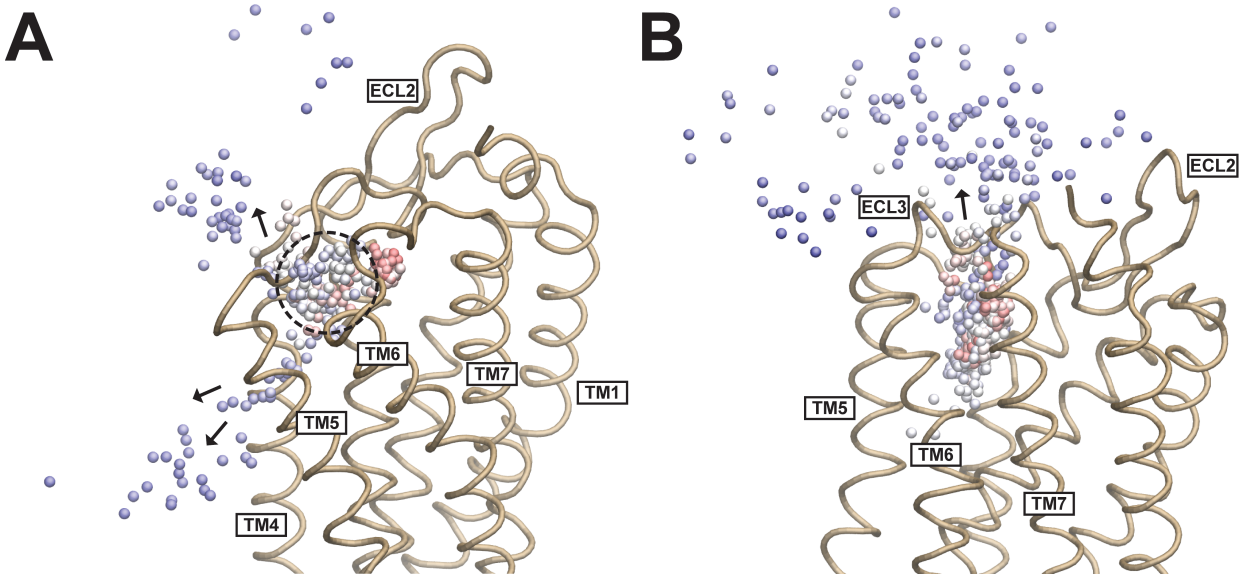

FIGURE S1. **Trajectories of vorapaxar COM during TAMD simulations of vorapaxar dissociation from PAR1.** The PAR1 backbone is shown as *light brown ribbons*. *Spheres* indicate the vorapaxar COM, and clusters of overlapping spheres represent metastable states. The simulation progresses from *red* to *white* to *blue*, with consecutive spheres representing 180 ps of simulation time. *Arrows* indicate the direction of vorapaxar motion. *A,* overlay of trajectories where vorapaxar exited between TMs 4 and 5. The metastable state is indicated by a *dashed circle*. *B*, overlay of trajectories where vorapaxar exited the extracellular face of the receptor.

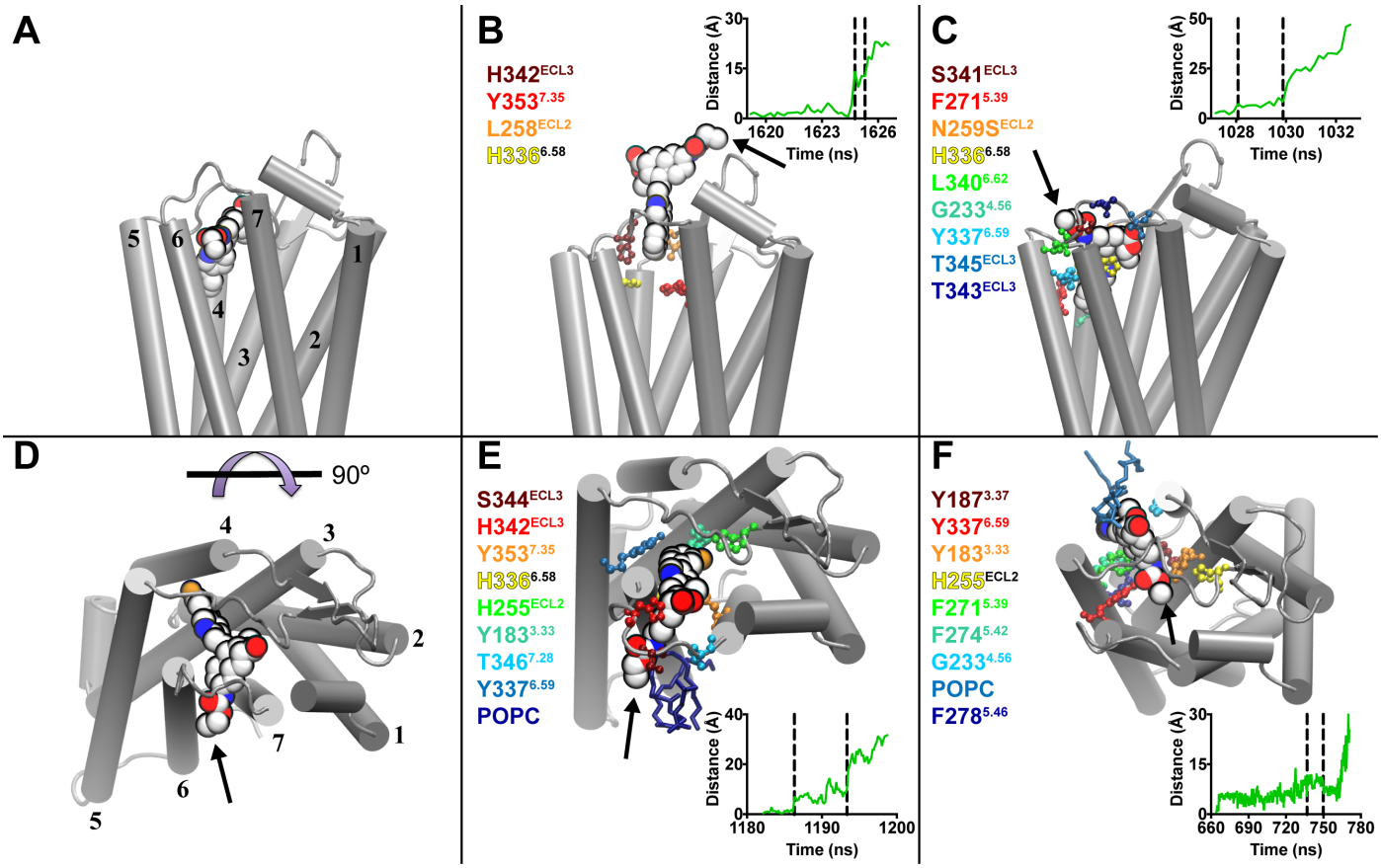

FIGURE S2. **Heterogeneity of metastable states prior to extracellular exit.** *A*, crystal structure of PAR1-vorapaxar as viewed from the plane of the lipid bilayer, looking toward TM6-7. TMs are shown as *cylinders* and labeled *1-7*. Vorapaxar is shown as *spheres*, and the ethyl carbamate moiety is indicated by an *arrow*. *B*, metastable state seen in one trajectory with vorapaxar interacting exclusively with ECL residues. *C*, metastable state seen in one trajectory with vorapaxar lying between ECL3 and the TM4-5 exit tunnel. *D*, extracellular view of the PAR1-vorapaxar crystal structure. View is rotated 90 degrees from that shown in *A*. *E,* metastable state with characteristics of TM6-7 exit observed prior to extracellular exit in one trajectory. *F*, metastable state with characteristics of TM4-5 exit observed prior to extracellular exit in one trajectory. Panels *B-C*, *E-F*, *Left*, the amino acid residues and POPC molecules that interact most frequently with vorapaxar in the metastable state are colored according to a heat map, from the most frequently interacting (*dark red*) to the ninth most frequently interacting (*dark blue*). Amino acids are rendered as *ball-and-stick* and lipids are rendered as *sticks*. Ballesteros-Weinstein numbering is indicated by *superscript*. Plots of the displacement of the vorapaxar COM from the crystallographic position versus simulation time are shown in the *top right* of panel *B-C* and the *bottom right* of panel *E-F*. The metastable state is indicated by *vertical dashed lines*. The metastable state shown in panel *B* was very brief and vorapaxar only interacted with four residues.

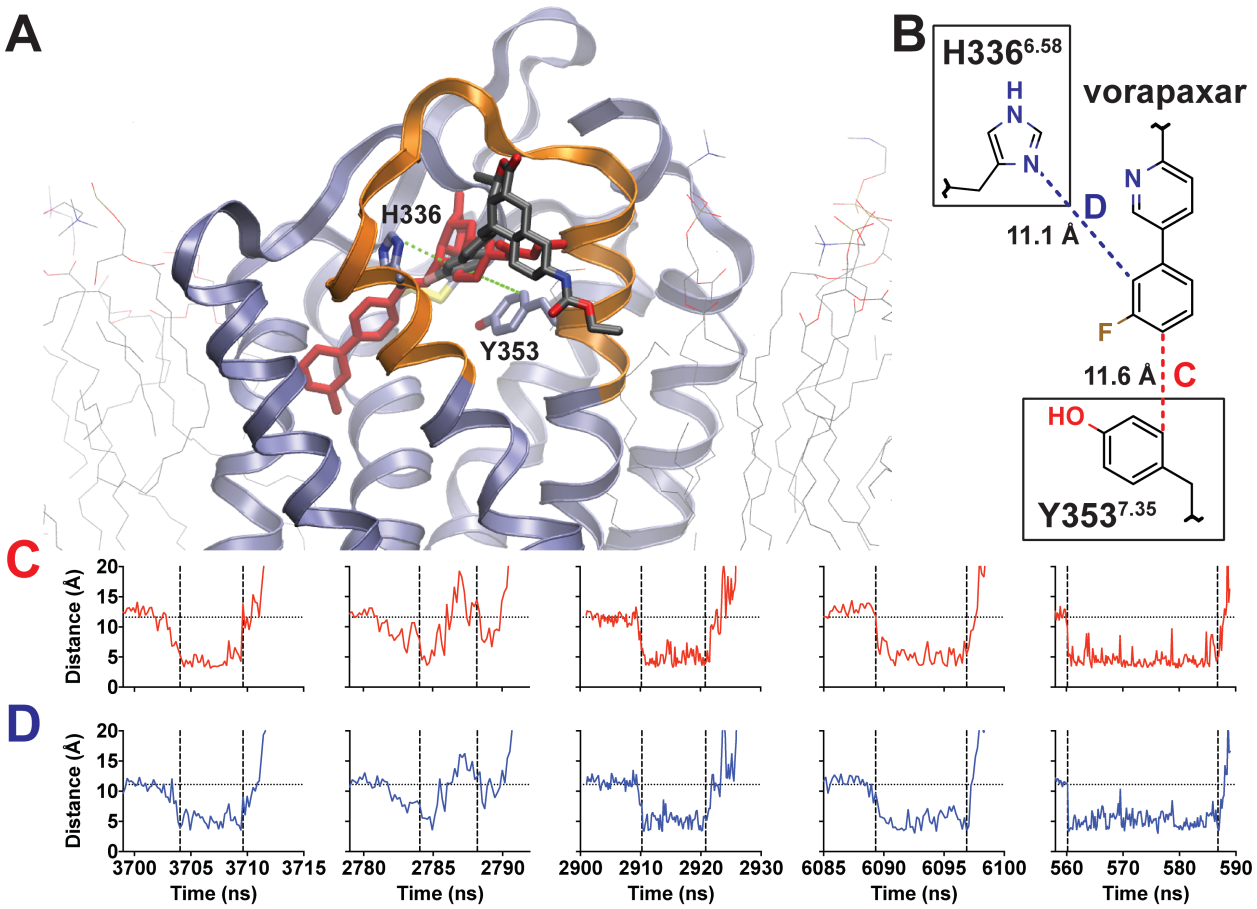

FIGURE S3. **Vorapaxar-PAR1 interactions in the TM6-7 metastable state.** *A,* frame from a TAMD simulation showing interactions of vorapaxar with residues H336$^{6.58}$ and Y353$^{7.35}$ in the metastable state. *Ribbons* PAR1, *orange ribbons* TM6-ECL3-TM7, *dark gray sticks* metastable position of vorapaxar, *red sticks* crystallographic position of vorapaxar, *blue sticks* H336$^{6.58}$ and Y353$^{7.35}$ side chains, *lines* POPC molecules in the simulation showing the position of the lipid bilayer, *green dashes* connect H336$^{6.58}$ and Y353$^{7.35}$ to the vorapaxar fluorophenyl ring. *B*, schematic showing the fluorophenyl moiety of vorapaxar and the crystallographic distances to H336$^{6.58}$ and Y353$^{7.35}$. *C*, distances from the vorapaxar fluorophenyl *para*- position to the *δ*-carbon of Y353$^{7.35}$ in each of five simulations where vorapaxar dissociated through the TM6-7 exit tunnel. This interaction is shown by the *red dashed line* in panel *B*. *D*, distances from the vorapaxar fluorophenyl *ortho*- position to the δ-nitrogen of H336$^{6.58}$ in the same five simulations. This interaction is shown by *blue dashed line* in panel *B*. The crystallographic distance is indicated by *horizontal dashed lines*, and the metastable state in each simulation is indicated by *vertical dashed lines*.

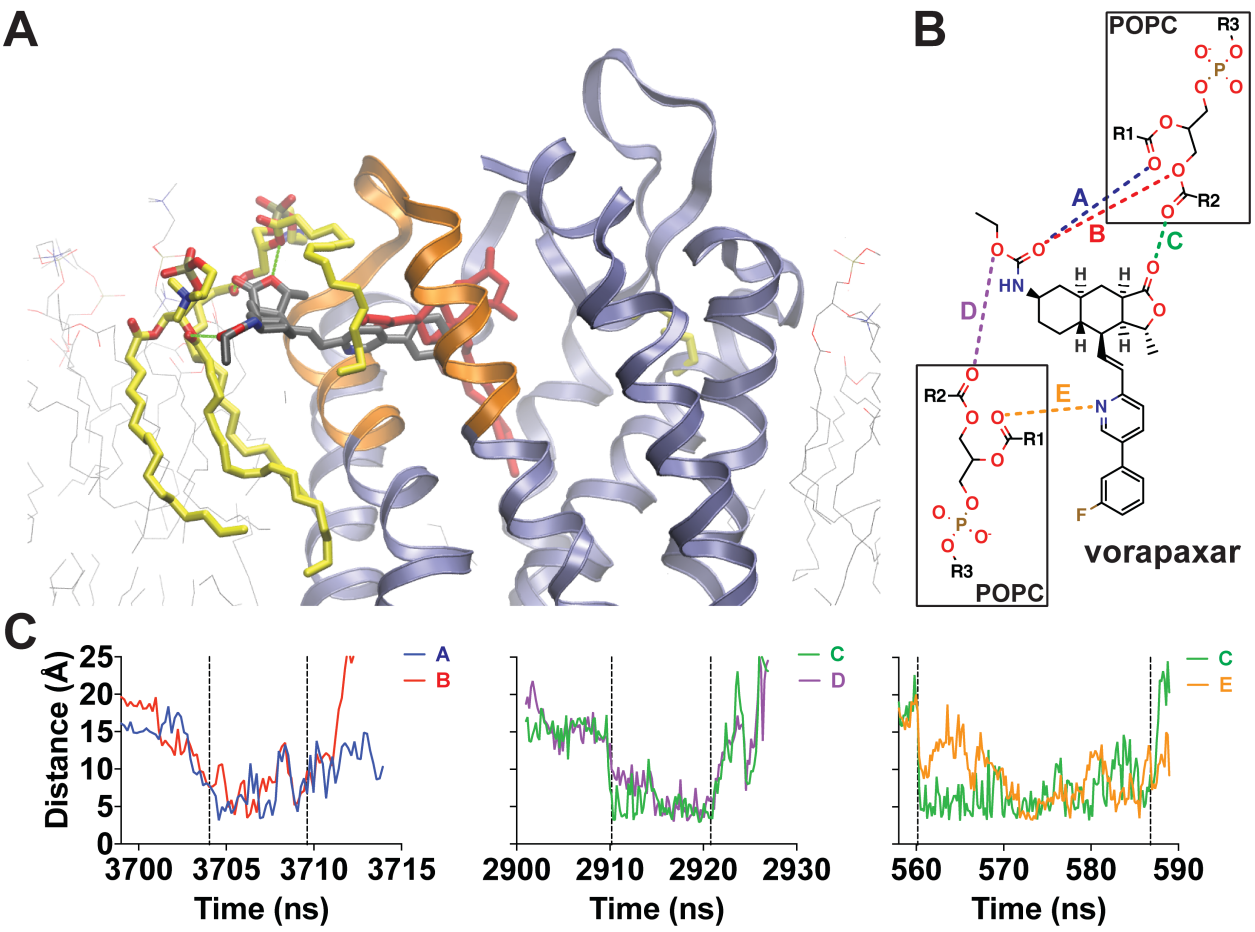

FIGURE S4. **Vorapaxar-lipid interactions in the TM6-7 metastable state.** *A*, frame from TAMD simulation showing interactions of vorapaxar with POPC molecules in the metastable state. *Ribbons* PAR1, *orange ribbons* TM6-ECL3-TM7, *dark gray sticks* metastable position of vorapaxar, *red sticks* crystallographic position of vorapaxar, *yellow sticks* POPC molecules interacting with vorapaxar, *lines* POPC molecules in the simulation showing the position of the lipid bilayer, *green dashes* polar interactions between vorapaxar and POPC ester groups. *B*, schematic showing polar interactions between vorapaxar and POPC head groups observed in simulations. *R1* and *R2* indicate POPC alkyl tails, and *R3* indicates choline. *C*, distances from vorapaxar polar atoms to the lipid head group oxygen atoms of the two most frequently interacting POPC molecules in each of three simulations. Labels and colors correspond to the interactions shown in panel *B*: (*A, blue,* and *B, red*) vorapaxar ethyl carbamate carbonyl oxygen to POPC, (*C, green*) vorapaxar methylfuranone carbonyl oxygen to POPC, (*D, magenta*) vorapaxar ethyl carbamate ester oxygen to POPC, and (*E, orange*) vorapaxar pyridine nitrogen to POPC. The metastable state in each simulation is indicated by *vertical dashed lines*.

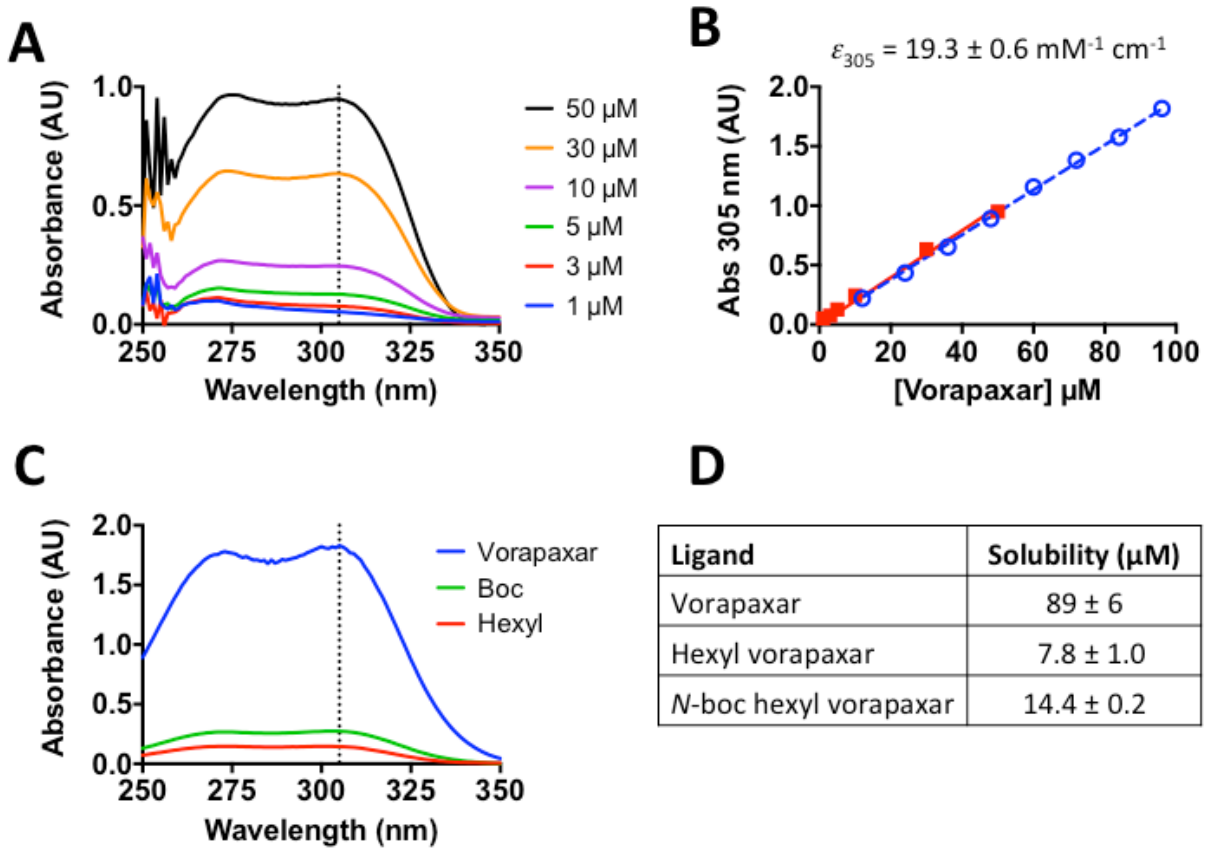

Ligand	Solubility (µM)
Vorapaxar	89 ± 6
Hexyl vorapaxar	7.8 ± 1.0
N-boc hexyl vorapaxar	14.4 ± 0.2

FIGURE S5. **UV absorption spectroscopy of vorapaxar.** *A,* example absorption spectra of vorapaxar in DMSO in the ultraviolet range. Dashed line indicates 305 nm. *B*, standard curve for determination of extinction coefficient (n = 2 independent experiments, *red* shows low-range dilutions in DMSO (1 to 50 µM), *blue* shows high-range dilutions in DMSO (10-100 µM). *C*, absorption spectra of solutions of clarified vorapaxar, *N*-boc-hexyl vorapaxar, and hexyl vorapaxar solutions after overnight incubation with 10 mM HPβCD in 10% DMSO / 90% water. *D*, solubility of vorapaxar and derivatives calculated using A305 (n = 3) in the HPβCD solution.

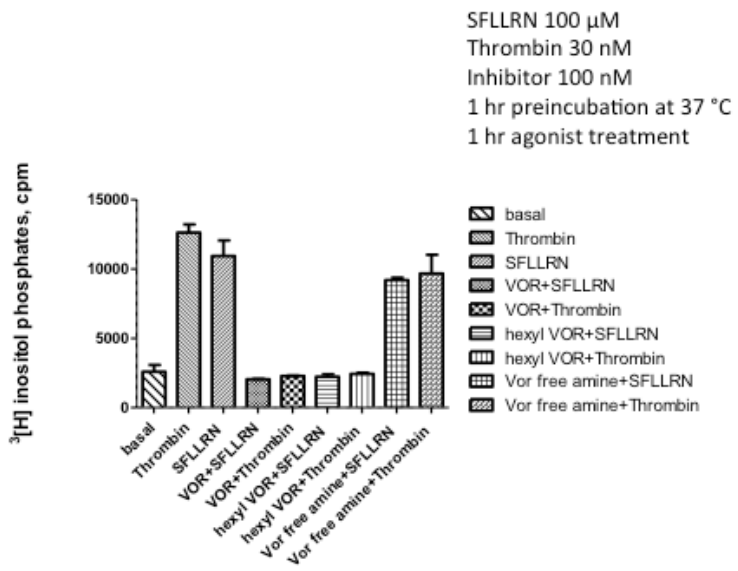

FIGURE S6. **Phosphoinositides accumulation assay.** Hexyl vorapaxar (hexyl VOR) and vorapaxar (VOR) are equally efficacious at preventing IP_3 release downstream of PAR1 stimulated by thrombin or SFLLRN.

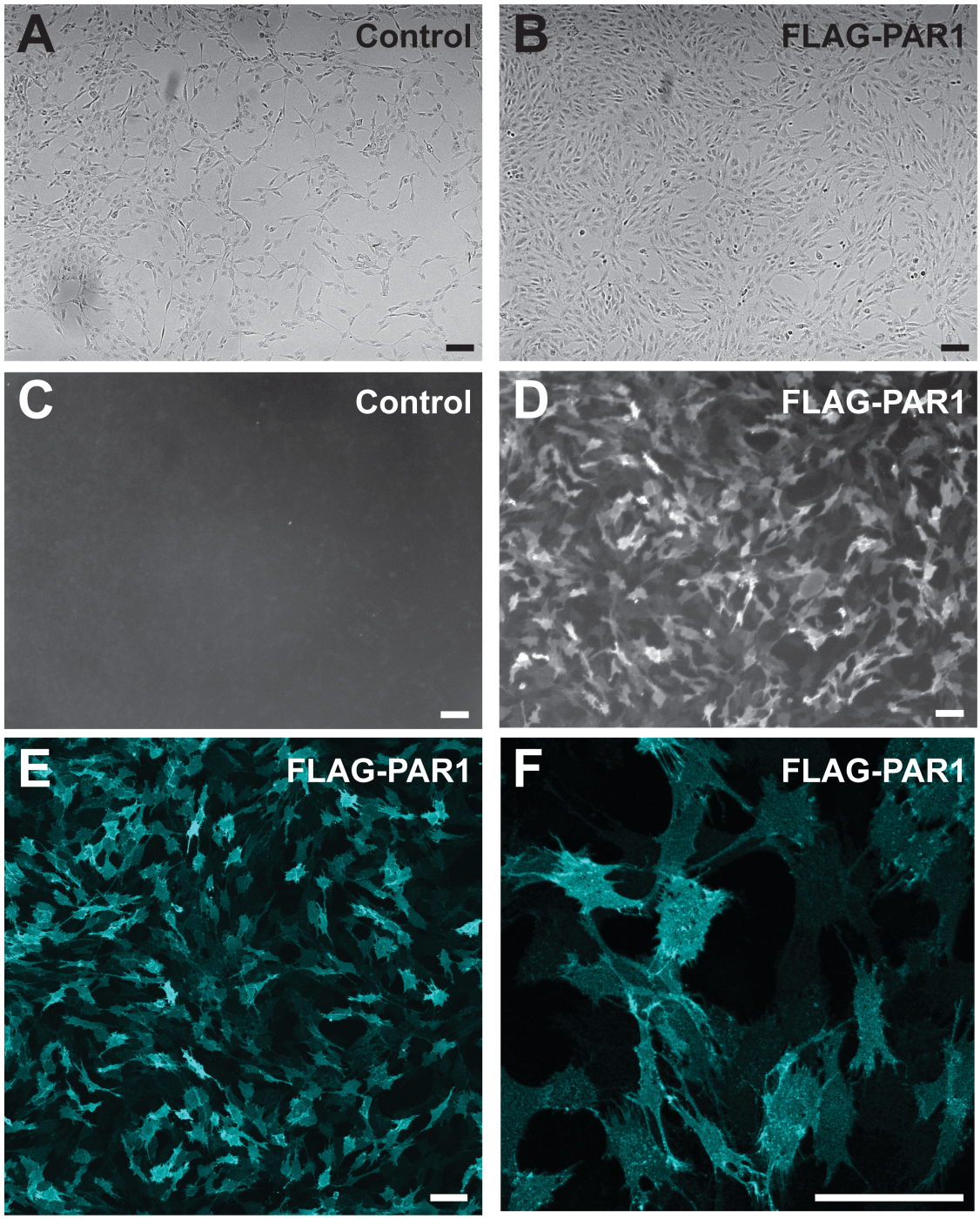

FIGURE S7. **Cell surface expression of N-terminally FLAG-tagged human PAR1 (hPAR1).** Fixed, unpermeabilized cells were stained with anti-FLAG M1 primary and Alexa488 secondary antibodies. *A-B,* brightfield images of Rat1 fibroblasts untransfected or stably transfected with hPAR1, respectively. *C-D,* epifluorescence images of the same fields. *E-F,* confocal images of stably transfected Rat1 fibroblasts at low and high magnification, respectively. *Scale bars* are 100 μm.

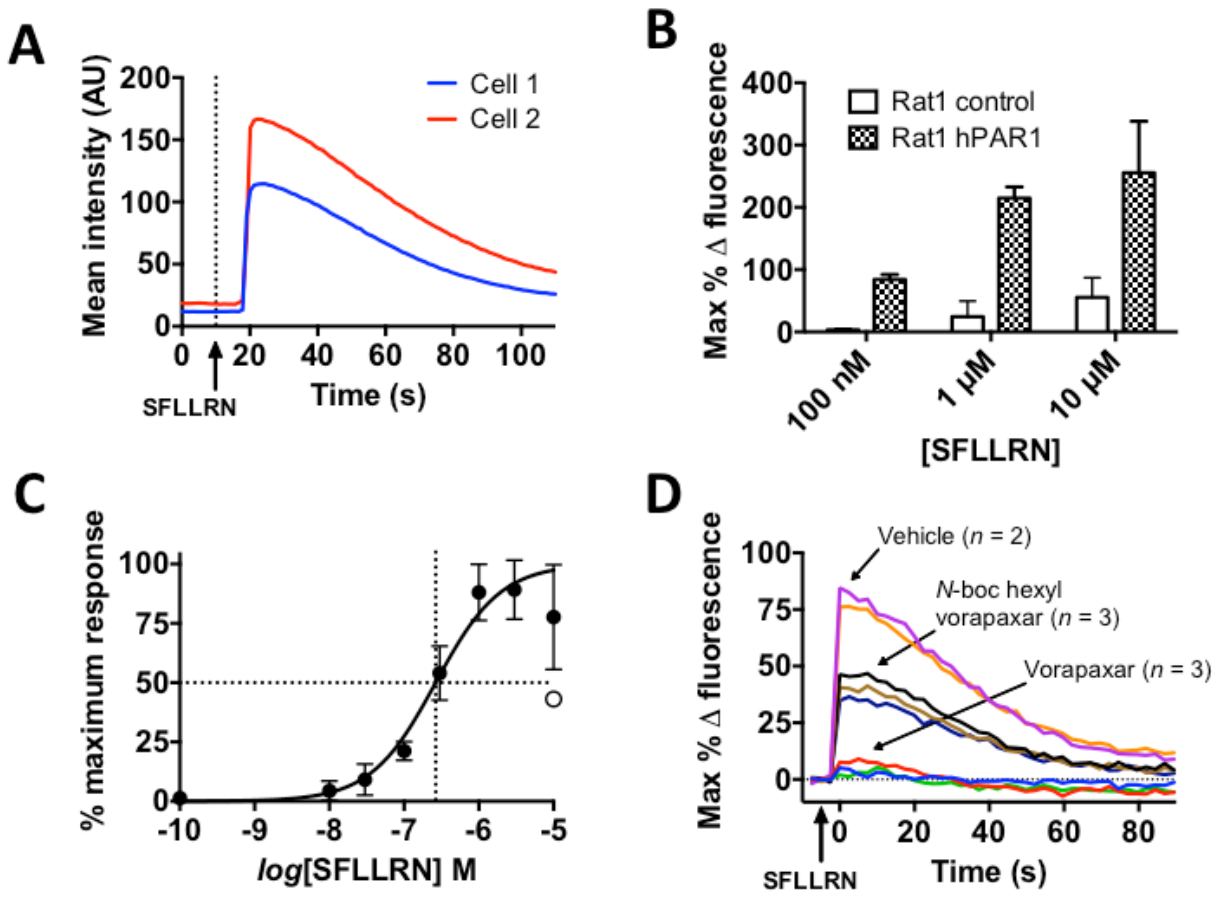

FIGURE S8. **Calcium flux inhibition assay of Rat1 fibroblasts stably expressing hPAR1.** *A,* typical single cell calcium transients as quantified by confocal microscopy in response to stimulation with 3 μM SFLLRN. *B,* coarse SFLLRN dose-response curve comparing control and hPAR1-overexpressing Rat1 fibroblasts (mean ± S.D. (*error bars*), n = 2-3 per bar). *C,* full dose-response curve for Rat1 fibroblasts stably overexpressing hPAR1 (mean ± S.D. (*error bars*), n = 5 wells per data point, one outlier shown as an open circle). Curve fitting results determined *log*EC50 = –6.58 ± 0.05 (mean ± std. error) for SFLLRN. *D,* example of calcium flux inhibition assay time point in 96-well format. After a 20 minute incubation, the vorapaxar-treated cells are almost completely inhibited, whereas the *N*-boc-hexyl vorapaxar-treated are partially inhibited. Agonist response was triggered by rapid addition of SFLLRN after baseline measurement. Note there is a discontinuity after agonist addition before reading out the agonist response due to ~5-10 sec lag time in startup of the 96-well plate reader.

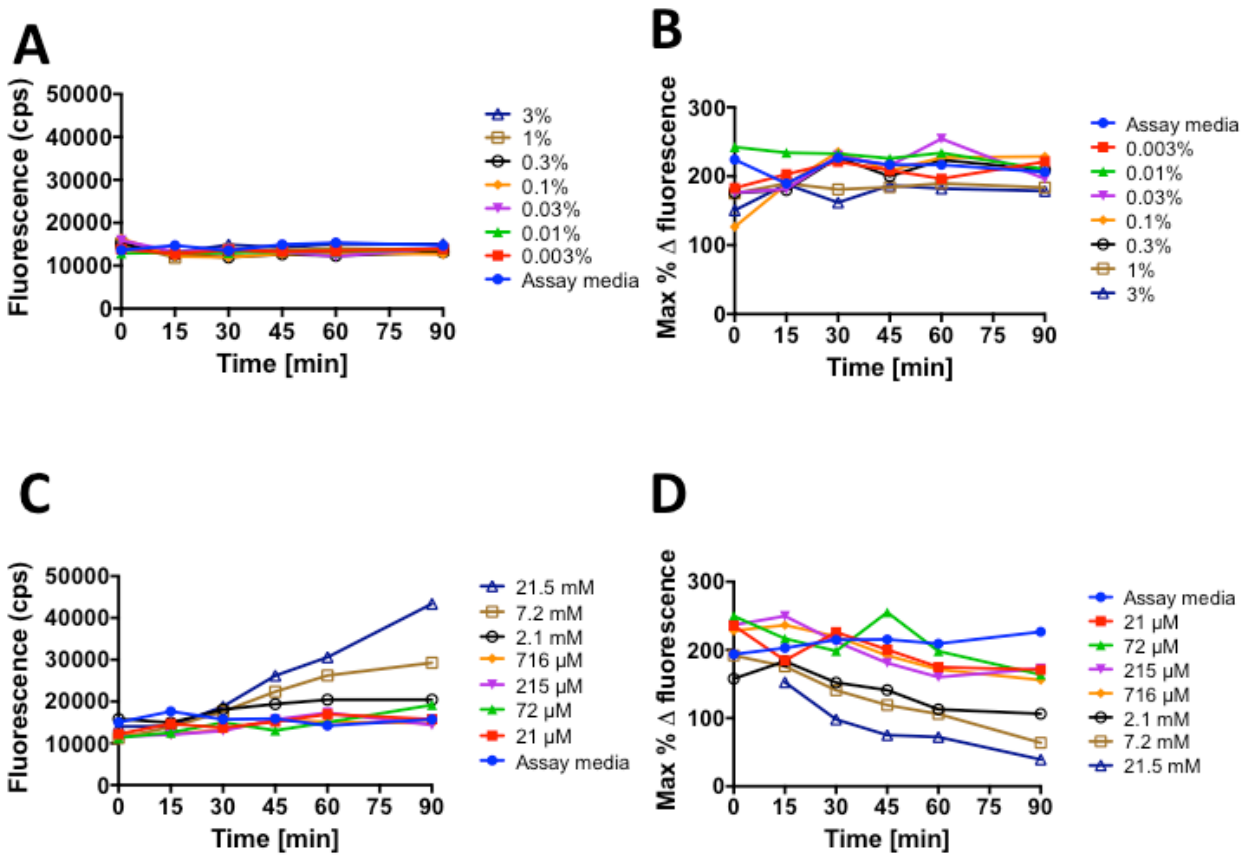

FIGURE S9. **Effect of vehicle on calcium fluorescence assay in Rat1 fibroblasts stably expressing hPAR1.** *A-B,* effect of DMSO on baseline fluorescence and peak response to 3 µM SFLLRN, respectively. *C-D,* effect of HPβCD on baseline fluorescence and peak response to 3 µM SFLLRN, respectively.

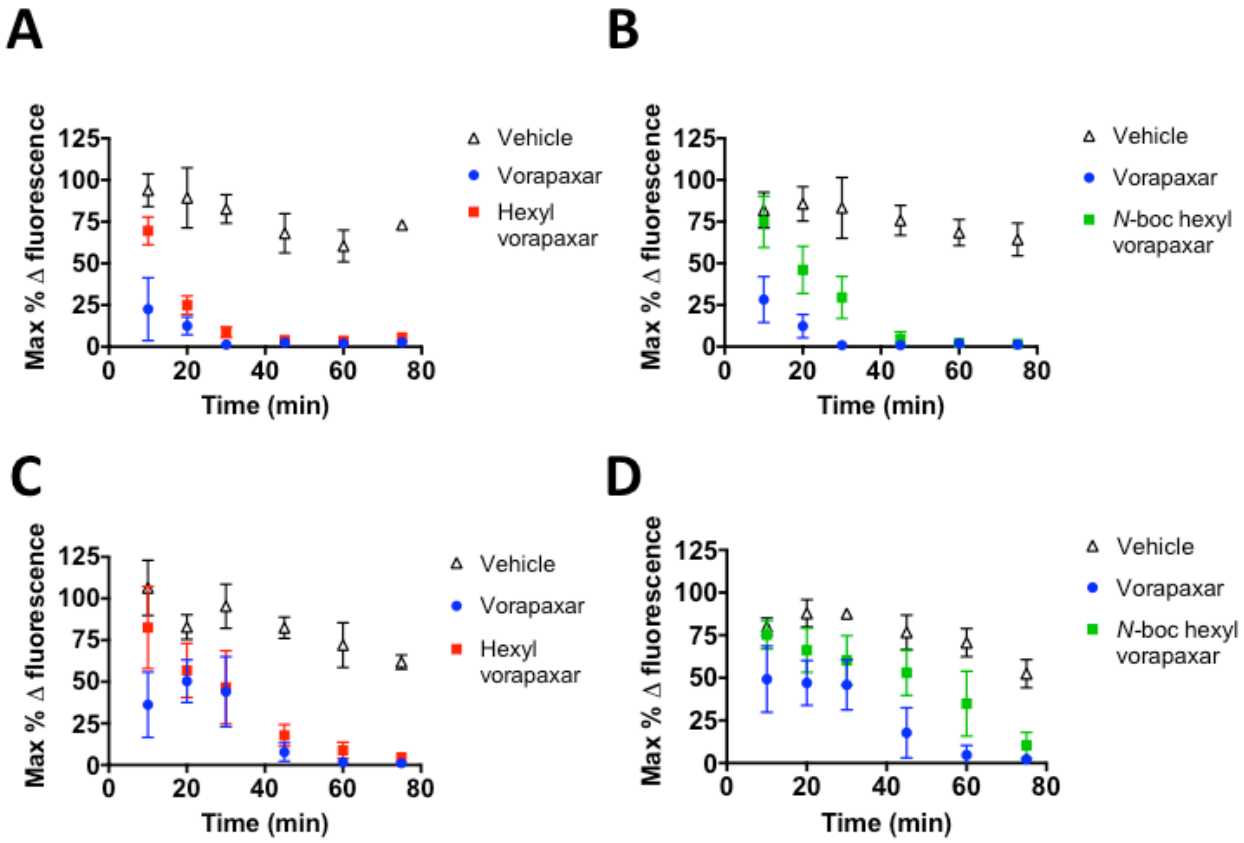

FIGURE S10. **Inhibition of calcium flux in response to 3 µM SFLLRN by vorapaxar derivatives in Rat1 fibroblasts stably expressing hPAR1.** All data points are mean ± S.D. (*error bars*). *A,* Head-to-head comparison of 1 µM vorapaxar (n = 3-6 per data point), hexyl vorapaxar (n = 3-6), and vehicle (n = 1-4). *B,* Comparison of 1 µM vorapaxar (n = 8-9 per data point), *N*-boc-hexyl vorapaxar (n = 8-9), and vehicle (n = 6). *C,* Comparison of 500 nM vorapaxar (n = 9 per data point), hexyl vorapaxar (n = 8-9), and vehicle (n = 5-6). *D*, Comparison of 500 nM vorapaxar (n = 9 per data point), *N*-boc-hexyl vorapaxar (n = 8-9), and vehicle (n = 6). Data set is representative of three independent experiments.

SUPPORTING MOVIE CAPTIONS

MOVIE S1. **Representative MD simulation of vorapaxar extracellular exit.** Movie corresponding to a clip of simulation time lasting 20 ns around the time of vorapaxar unbinding from PAR1 via an extracellular pathway (corresponds to Supporting Fig. 2*E*). PAR1 TMs are shown as *gray cylinders*, loops as *gray ribbons*, and amino acids as *ball-and-stick*. Vorapaxar is shown as *spheres,* and a lipid is shown as *dark blue sticks*. The amino acid residues and POPC molecule that interact most frequently with vorapaxar are colored as follows (from the most frequently interacting to the ninth most frequently interacting): S344^{ECL3} (*dark red*), H342^{ECL3} (*bright red*), Y353$^{7.35}$ (*orange*), H336$^{6.58}$ (*yellow*), H255^{ECL2} (*bright green*), Y183$^{3.33}$ (*sea foam green*), T346$^{7.28}$ (*turquoise*), Y337$^{6.59}$ (*medium blue*), and POPC (*dark blue*).

MOVIE S2. **Representative MD simulation of vorapaxar exit through TM6-7.** Movie corresponding to a clip of simulation time lasting 30 ns around the time of vorapaxar unbinding from PAR1 via a TM6-7 pathway (corresponds to Figure 3*F*). PAR1 TMs are shown as *gray cylinders*, loops as *gray ribbons*, and amino acids as *ball-and-stick*. Vorapaxar is shown as *spheres,* and lipids are shown as *sticks*. The amino acid residues and POPC molecules that interact most frequently with vorapaxar are colored as follows (from the most frequently interacting to the ninth most frequently interacting): POPC (*dark red*), Y353$^{7.35}$ (*bright red*), POPC (*orange*), H336$^{6.58}$ (*yellow*), L332$^{6.54}$ (*bright green*), A349$^{7.31}$ (*sea foam green*), Y350$^{7.32}$ (*turquoise*), POPC (*medium blue*), and T345^{ECL3} (*dark blue*).

MOVIE S3. **Representative MD simulation of vorapaxar exit through TM4-5.** Movie corresponding to a clip of simulation time lasting 60 ns around the time of vorapaxar unbinding from PAR1 via a TM4-5 pathway (corresponds to Figure 4*D*). PAR1 TMs are shown as *gray cylinders*, loops as *gray ribbons*, and amino acids as *ball-and-stick*. Vorapaxar is shown as *spheres*. The amino acid residues that interact most frequently with vorapaxar are colored as follows (from the most frequently interacting to the ninth most frequently interacting): Y187$^{3.37}$ (*dark red*), G233$^{4.56}$ (*bright red*), F278$^{5.46}$ (*orange*), Y353$^{7.35}$ (*yellow*), Y337$^{6.59}$ (*bright green*), L229$^{4.52}$ (*sea foam green*), F271$^{5.39}$ (*turquoise*), L262^{ECL2} (*medium blue*), and Q242^{ECL2} (*dark blue*).

MOVIE S4. **Calcium flux induced by PAR1 agonist SFLLRN.** Calcium transients were recorded from Rat1 fibroblasts stably transfected with human PAR1 using time-resolved confocal microscopy (see *Methods*). Frames were captured every 500 ms using Fluo4 filters. Movie is accelerated 10-fold (1 s of movie time = 10 s of experiment time, total experiment length = 100 s). At t = 10 s of experimental time,

corresponding to t = 1 s of movie time, the PAR1 agonist peptide SFLLRN was rapidly diluted into the chamber to a final concentration of 1 μM. The field of view is 640 μm x 640 μm.